The Boron conundrum: The case of cationic clusters B n +with n = 2–20

3 AUTHORS:

Truong Tai
University of Leuven
67 PUBLICATIONS **524** CITATIONS

SEE PROFILE

Tam Minh Nguyen
University of Leuven
20 PUBLICATIONS **140** CITATIONS

SEE PROFILE

Minh Tho Nguyen
University of Leuven
750 PUBLICATIONS **11,206** CITATIONS

SEE PROFILE

REGULAR ARTICLE

The Boron conundrum: the case of cationic clusters B_n^+ with $n = 2$–20

Truong Ba Tai · Nguyen Minh Tam · Minh Tho Nguyen

Abstract We investigate the molecular and electronic structure and thermochemical properties of the cationic boron clusters B_n^+ with $n = 2$–20, using both MO and DFT methods. Several functionals are used along with the MP2, G3, G3B3, G4, and CCSD(T)/CBS methods. The latter is the high accuracy reference. While the TPSS, TPSSh, PW91, PB86, and PBE functionals show results comparable to high-accuracy MO methods, both BLYP and B3LYP functionals are not accurate enough for three-dimensional (3D) structures. A negligible difference is observed between the B3LYP, MP2, and CCSD(T) geometries. A transition between 2D and 3D structures occurs for this series at the B_{16}^+–B_{19}^+ sizes. While smaller clusters B_n^+ with $n \leq 15$ are planar or quasi-planar, a structural competition takes place in the intermediate sizes of B_{16-19}^+. The B_{20}^+ cation has a 3D tubular shape. The standard heats of formation are determined and used to evaluate the cluster stability. The average binding energy tends to increase with increasing size toward a limit. All closed-shell species B_n^+ has an aromatic character, but an enhanced stability is found for B_5^+ and B_{13}^+ whose aromaticity and electron delocalization are analyzed using the LOL technique.

T. B. Tai · N. M. Tam · M. T. Nguyen (✉)
Department of Chemistry, University of Leuven,
3001 Leuven, Belgium
e-mail: minh.nguyen@chem.kuleuven.be

N. M. Tam
Institute for Computational Science and Technology (ICST),
HoChiMinh City, Vietnam

1 Introduction

Boron-based clusters continue to be a subject of considerable theoretical and experimental interests. Extensive investigations have been performed on small boron clusters using various theoretical and experimental methods [1–25]. While there is a good agreement for the electronic structure and chemical properties of small boron clusters B_n with $n \leq 13$ in the recent literature [26, 27], those of the larger clusters are still a matter of controversy [11, 19, 28, 29]. Such a discrepancy almost arises from the fact that the computational methods used in previous studies differ much from each other. For instance, most of the recent studies on small boron clusters were performed using the density functional theory (DFT), but with a variety of functionals [27]. Although many theoretical predictions based on the popular hybrid B3LYP functional were found in good agreement with available experimental results [27], it has been claimed in other reports that this functional is not reliable for boron clusters. Based on calculated results for the twenty-atom clusters $B_{20}^{0/-}$, An et al. [30] argued that the PBE0 functional behaves better than the B3LYP, as compared to the perturbation theory (MP4) and coupled-cluster (CCSD(T)) results. Pan et al. [31] also claimed that the B3LYP functional is not reliable for relative energies of three-dimensional structures. The latter authors reported that the PBE, TPSS, and TPSSh functionals provide energetic parameters for B-compounds more comparable to the CCSD(T) counterparts. More recently, Li et al. [32] reexamined the structures of B_{20} using the molecular orbital

(MO) methods at the CCSD(T)/6-311G(d)//MP2/6-311G(d) level along with eight different density functionals, including the BLYP, B3LYP, PBE, PBE0, TPSS, TPSSh, mPW1PW91, and M06-2X. Their calculated results pointed out that the relative energies of B_{20} isomers obtained from PBE and TPSS functionals are closer to the CCSD(T) values than those obtained from other functionals. In this context, a calibration of the accuracy of various computational methods, in particular of the less popular density functionals, needs to be done carefully.

The cationic boron clusters have been the subject of several experimental investigations. For instance, Anderson et al. [1, 2] performed experimental investigations on small cationic boron clusters B_n^+ ($n = 2–13$) using the absolute collision-induced dissociation (CID) technique. Measurements of fragment appearance potentials and fragmentation branching ratios were carried out, and the obtained data were analyzed to interpret the stabilities of the ionic clusters along with the ionization energies (IEs) of the corresponding neutrals. Recently, a combined experimental and theoretical study on larger cationic boron clusters B_n^+ with $n = 12–25$ was also carried out by Oger et al. [28]. In this report, the collision cross sections of the low-lying isomers B_n^+ were obtained by using DFT calculations and compared to the experimental data based on ion mobility spectrometry.

According to our best knowledge, while a number of theoretical studies on small cationic clusters B_n^+ with $n = 2–14$ were carried out [33–47], investigations on the larger clusters are rather limited [28, 29]. Moreover, as stated above, the identity of the global minima of B_n^+ clusters (being the most stable isomeric forms) remains a matter of debate. Let us mention the cationic B_6^+ cluster as a case in point. At the MP2/6-311G(d) level, Li et al. [43] found that the B_6^+ ion exhibits a C_{2h} ^2B_g global minimum. Using DFT methods, Ma et al. [44] indicated instead a high symmetry D_{2h} $^2B_{1u}$ structure to be the most stable isomer for B_6^+. While Ray et al. [33] subsequently claimed that the global minimum B_6^+ is a square pyramid, a perfect hexagonal structure was reported as its lowest-energy isomer by Niu et al. [35]. Another C_2 structure was also indicated to be the most stable B_6^+ isomer by Kato et al. [34]. Similar stories can be told for other sizes such as B_5^+, B_7^+, B_8^+, B_9^+, and B_{13}^+ [33–35, 38, 39, 45–47]. More interestingly perhaps is the fact that the transition between 2D and 3D structures has been assumed to occur at the cation B_{16}^+ following a combined experimental and theoretical study by Oger et al. [28]. Accordingly, the cationic clusters B_n^+ with $n = 17–25$ were found to possess tubular structures, similar to the tubular B_{20} [11], while the B_{16}^+ has a caged form. However, a recent report by Boustani et al. [29] pointed out that the B_{19}^+ ion has rather a 3D pyramid structure. These discrepancies,

typical of the *boron conundrum*, require the identity of the molecular structures of the B_n^+ clusters to be reliably established.

We recently performed the theoretical investigations of thermochemical properties and electronic structures of small boron clusters B_n ($n = 2–13$) in both neutral and anionic states [17, 18, 26], and of the larger neutral clusters B_n with n up to 20 [20] using high-accuracy molecular orbital G3B3 and CCSD(T)/CBS methods. Our theoretical predictions are in good agreement with the available experimental results. In addition, our calculated results allowed different aspects of their bonding and growth pattern to be understood. Some non-classical types of bonding and aromaticity have been discovered [20]. Motivated by the above reasons, we now continue our investigations on the cationic boron clusters B_n^+ with $n = 2–20$. The calibration of computational methods used is done carefully by using various methods, including MP2, G3, G4, CCSD(T), and CBS, and seven different density functionals. Thermochemical properties are determined using the G3B3 and CCSD(T)/CBS methods.

2 Computational methods

All quantum chemical calculations are carried out using the Gaussian 03 [48] and Molpro 2008 [49] suites of programs. The initial search for all possible lower-lying isomers of each of the B_n^+ clusters considered is performed using a stochastic search algorithm that was implemented by us [50]. Firstly, the possible structures of each of the clusters B_n^+ are generated by a random kick method and then rapidly optimized at the B3LYP/6-31G level [51]. In this search procedure, the minimum and maximum distances between atoms are limited to 1.5 and 9 Å, respectively. Geometries of the stationary points located and their harmonic vibrational frequencies are further refined using the B3LYP functional, initial part of the composite G3B3 approach [52], for the series of small clusters B_n^+ with $n = 2–13$. For the series of larger sizes of $n = 14–20$, geometry optimizations and vibrational calculations are performed using the B3LYP [53–55] and PBE [56] functionals in conjugation with the 6-311+G(d) basis set [57]. Their single-point electronic energies are subsequently calculated using the coupled-cluster CCSD(T) theory [58] at their B3LYP optimized geometries.

In order to obtain more accurate energetic values, the electronic energies of the global minima are calculated using the coupled-cluster CCSD(T) theory at the complete basis set limit (CBS) for the small sizes of $n = 2–8$, and the composite G3B3 technique for all B_n^+ clusters considered (with $n = 2\_20$). Geometrical parameters are also fully optimized at the coupled-cluster CCSD(T) theory for

the small sizes of $n = 2$–8, in conjunction with the correlation-consistent aug-cc-pVTZ basis set.

A detailed description for the CCSD(T)/CBS approach is found elsewhere [26, 59–61]. Briefly, the single-point electronic energies are calculated by using the restricted/unrestricted coupled-cluster R/UCCSD(T) formalism [62–64] and extrapolated to the complete basis set limit (CBS) based on the correlation-consistent aug-cc-pVnZ (n = D, T, and Q) basis sets [65, 66]. The CCSD(T) energies are then extrapolated to the CBS limit energies using expression (1) [67]:

$$E(x) = A_{CBS} + B \exp[-(x - 1)] + C \exp[-(x - 1)]^2 \quad (1)$$

where x = 2, 3, and 4 for the aug-cc-pVnZ basis sets with n = D, T, and Q, respectively.

The zero-point energies (ZPE) are calculated from harmonic vibrational frequencies at either the CCSD(T)/aug-cc-pVTZ or the MP2/aug-cc-pVTZ level. Additional smaller corrections are included in the evaluation of total atomization energies (TAE). Core-valence corrections (ΔE_{CV}) are obtained at the CCSD(T)/cc-pwCVTZ level [68, 69]. Douglas–Kroll–Hess (DKH) scalar relativistic corrections (ΔE_{DKH-SR}), which account for changes in the relativistic contributions to the total energies of the molecule and the constituent atoms, are calculated using the spin-free, one-electron DKH Hamiltonian [70–73]. ΔE_{DKH-SR} is defined as the difference in the atomization energy between the results obtained from basis sets recontracted for DKH calculations and the atomization energy obtained with the normal valence basis set of the same quality. The DKH calculations are obtained as the differences of the results from the CCSD(T)/cc-pVTZ and the CCSD(T)/cc-pVTZ-DK levels of theory. Finally, a spin–orbit (SO) correction of 0.03 kcal/mol for the B-atom obtained from the excitation energies of Moore [74] is used. The total atomization energy (ΣD_0 or TAE) of a compound is given by (2):

$$\Sigma D_0 = \Delta E_{elec}(CBS) + \Delta E_{CV} + \Delta E_{DKH-SR} + \Delta E_{SO} - \Delta E_{ZPE} \quad (2)$$

By combining our computed ΣD_0 values from either the CBS or G3B3 calculations, with the known heat of formation at 0 K for the element B, we can derive the heats (enthalpies) of formation $\Delta_f H°$ values at 0 K for the molecules in the gas phase. In this work, we use the value of $\Delta_f H°$(B) = 135.1 ± 0.2 kcal/mol [75], and the rationale for this selection was discussed in our previous work [26, 76–78]. The heats of formation at 298 K are obtained by following the usual thermochemical procedures [79]. The calculated heats of formation at 0 K are used to evaluate the ionization energies and other energetic quantities.

In a further step to evaluate the accuracy of the computational approaches used, the relative energies of B_6 isomers are calculated using a series of different methods, including the MP2, G3 [80], G3B3 [52], G4 [81], CCSD(T)/CBS, and seven different density functional including BLYP [54, 82], B3LYP [41], TPSS [83], TPSSh [84, 85], PBE [56], BP86 [86], and PW91 [87]. The B_6 is chosen as a sample for calibration because of two reasons: first, there exist several stable isomers B_6, including the planar, quasi-planar, and three-dimensional structures as shown in Fig. 1. Second, it is simply due to the fact that B_6 is small enough to allow the demanding methods such as CCSD(T)/CBS to be performed within our computational resources.

3 Results and discussion

3.1 Evaluation of computational methods

The relative energies of B_6 isomers obtained from various methods are given in Table 1, while the illustrating plots are shown in Fig. 2. There is a consistency between high-accuracy theoretical methods such as G3, G3B3, G4, CCSD(T)/aug-cc-pVTZ, and CCSD(T)/CBS (Fig. 2a). The relative energies obtained from the simpler MP2 method are much different as compared to those obtained from the above methods. The MP2 method tends to favor three-dimensional (3D) caged structures. Figure 2a shows that the MP2 relative energies of 3D structures **II** and **III** are much lower than those obtained from CCSD(T) and other methods, while the MP2 relative energies of two-dimensional (2D) structures **IV**, **V,** and **VI** become considerably higher.

Interestingly, all density functionals considered present the energy values approximately close for planar or quasi-planar closed-shell structures, that are also in good agreement with the relevant CCSD(T)/CBS values. However, for 3D structures, the B3LYP and BLYP results turn out to be less accurate as compared to other functionals, relative to the CBS values. Opposite to the MP2, the two latter
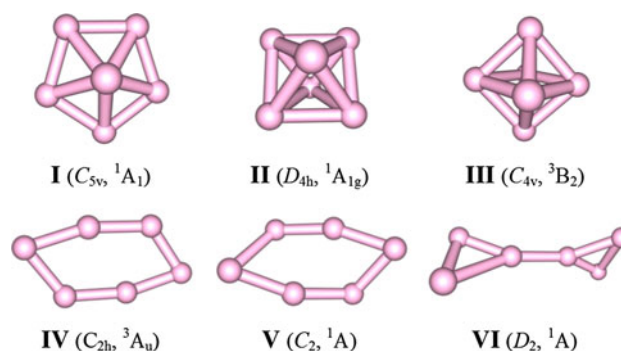

Fig. 1 Shapes of the lower-lying isomers of B_6

Table 1 Relative energies (kcal/mol) of the low-lying isomers B_6 obtained at various computational methods

Method	I	II	III	IV	V	VI
CBS[a]	0.0	40.8	37.9	7.7	10.2	56.7
G3	0.0	36.3	36.4	5.8	6.1	50.0
G3B3	0.0	38.0	36.4	6.2	6.4	50.2
G4	0.0	35.9	34.4	8.9	9.0	52.7
MP2/6-311+G(d)	0.0	23.8	18.6	11.6	17.9	57.9
CCSD(T)/aug-cc-pVTZ	0.0	41.2	38.3	5.9	8.2	53.0
CCSD(T)/6-311+G(d)	0.0	41.3	38.5	3.8	5.8	48.5
CCSD(T)/MP2[b]	0.0	36.9	38.5	4.2	6.3	48.5
CCSDT/B3LYP[c]	0.0	41.2	38.6	3.8	6.4	48.4
B3LYP/6-311+G(d)[d]	2.7	59.2	43.3	0.0	9.2	63.2
BLYP/6-311+G(d)	5.2	54.3	41.3	0.0	6.0	55.3
TPSS/6-311+G(d)	2.1	45.1	27.8	0.0	11.3	64.2
TPSSh/6-311+G(d)	1.4	47.7	29.3	0.0	13.1	67.5
PBE/6-311+G(d)	0.0	39.8	24.4	0.7	9.6	62.8
PW91/6-311+G(d)	0.6	42.1	26.7	0.0	9.2	62.5
BP86/6-311+G(d)	1.2	44.2	29.5	0.0	8.3	60.0

[a] CBS energy calculated from the CCSD(T)/aug-cc-pVnZ energies (n = D, T, Q) with the CCSD(T)/aug-cc-pVTZ geometries

[b] CCSD(T) single-point energy calculated at the MP2 geometries with the 6-311+G(d) basis set

[c] CCSD(T) single-point energy calculated at the B3LYP geometries with the 6-311+G(d) basis set

[d] DFT energy values included the zero-point energies (ZPEs)

functionals do not favor 3D structures as shown in Fig. 2b. These observations agree well with the recent reports [30–32]. In addition, the relative energies of open-shell species obtained from DFT methods are smaller than the corresponding CCSD(T)/CBS values.

In order to evaluate further the accuracy of the methods used, electronic energies of the isomers are further calculated using the CCSD(T) method with the B3LYP, MP2, and CCSD(T) optimized geometries. The results plotted in Fig. 2c point out that there is a remarkably good agreement between the CCSD(T) values with three different geometries. Thus, we can conclude that the use of geometries of isomers optimized by different methods induce a negligible difference in their relative energies. The difference in relative energies is mainly due to the electronic energies of the methods used.

3.2 Shape of the low-lying isomers of cationic B_n^+ clusters

Shapes, relative energies, number of imaginary frequencies, symmetry point group, and electronic states of lower-lying isomers B_n^+ are depicted in Figs. 3, 4, and 5.

B_2^+, B_3^+, and B_4^+ Our calculated results agree well with the earlier reports [33–39, 88] that the structures **2.1** ($D_{\infty h}$, $^2\sum_g^+$), **3.1** (D_{3h}, $^1A_1'$), and **4.1** (D_{2h}, ^2A_g) are the global minima of B_2^+, B_3^+, and B_4^+, respectively. These

structures have almost the same shapes as their neutral counterparts.

B_5^+ As stated above, there is a controversy about the global minimum of B_5^+. Anderson et al. [2] and Ray et al. [33] reported that the most stable isomer of B_5^+ is a trigonal bipyramid structure **5.2**. Subsequent studies are in agreement with each other that the B_5^+ ion possesses a C_{2v} structure **5.1**, being distorted form of high symmetry D_{5h} [27, 34, 40, 42]. Our calculated results concur with the latter results. **5.1** can thus be established as the lowest-energy isomer of B_5^+, while **5.2** is found to be 51.4 kcal/mol less stable than the **5.1**.

B_6^+ As discussed above, due to the use of different theoretical methods, there is also a discrepancy in the results for the global minimum B_6^+ reported in the literature. Let us briefly mention again the reported results. At the MP2/6-311G(d) level, Li et al. [43] showed that the B_6^+ exhibits the C_{2h} ^2B_g global minimum **6.3**. Using DFT calculations, Ma et al. [44] and Rica et al. [40] indicated the high symmetry D_{2h} $^2B_{1u}$ structure **6.1** to be the most stable isomer for B_6^+. While Ray et al. [33] claimed that the B_6^+ global minimum is a square pyramid structure **6.4**, a perfect hexagonal structure was reported by Niu et al. [35] as the most stable isomer. Two other structures, including a capped pentagonal **6.2** and a C_2 structure, were also suggested to be the most stable isomers of B_6^+ by Hanley et al. [2] and Kato et al. [34], respectively.
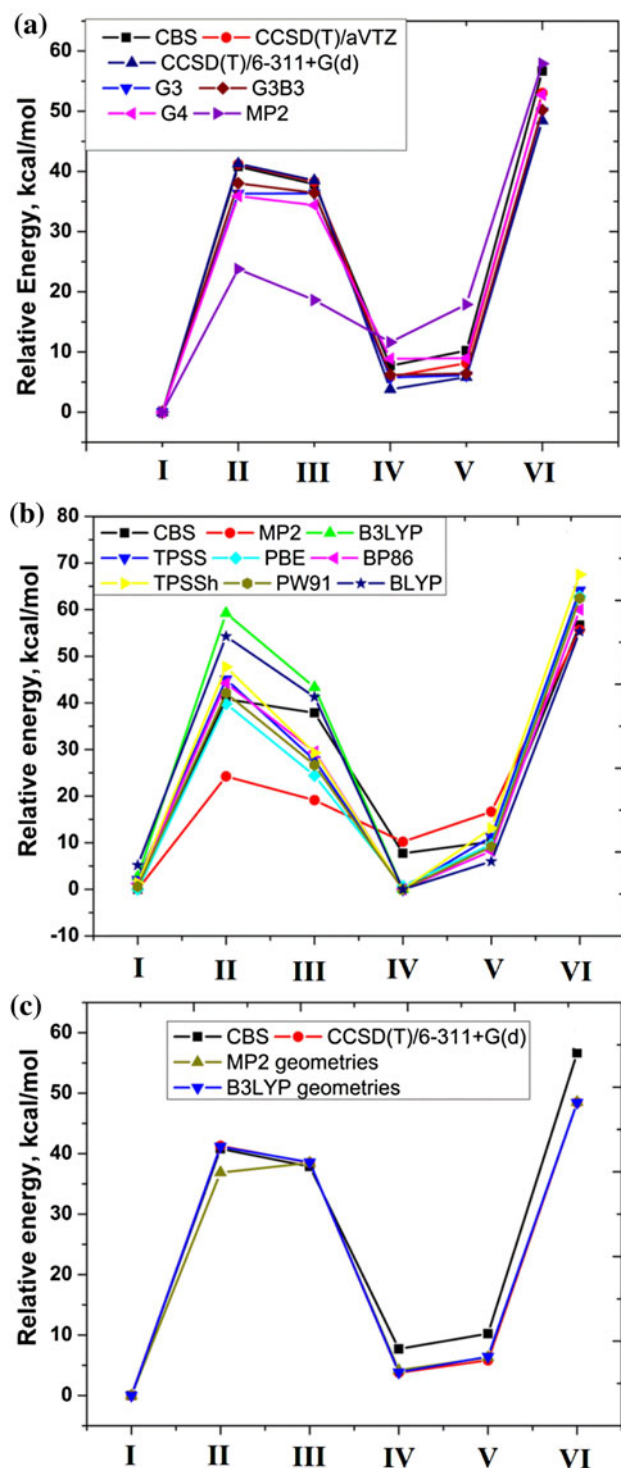
Fig. 2 The curves of relative energies (kcal/mol) of the lower-lying B_6 isomers obtained using various computational methods

To gain additional insights, we reexamine the energies of all above structures using both G3B3 and CCSD(T)/aug-cc-pVTZ methods. Our calculations point out that the two structures **6.1** (D_{2h} $^2B_{1u}$) and **6.2** (C_s $^2A'$), which is a distorted form of the neutral B_6, are almost degenerate in energy (Fig. 3). The energy difference between them amounts to only 0.7 and 1.0 kcal/mol at the G3B3 and CCSD(T) levels of theory, respectively. The C_{2h} ^2B_g structure **6.3** is only a transition state with one imaginary frequency connecting **6.1**, and a relative energy of 7.8 kcal/mol at the CCSD(T) level (5.7 kcal/mol at G3B3). **6.4** that was reported to be the global minimum by Ray et al. [33] was also located, but it is now found to be much less stable with a relative energy of 27.7 kcal/mol.

B_7^+ Our calculations concur with the recent reports [34, 36, 38, 39] that the C_{6v} $^1A_1$ structure **7.1** is the global minimum of B_7^+. Although another structure with bipyramid pentagonal shape was reported as the B_7^+ global minimum, it turns out to be much less stable.
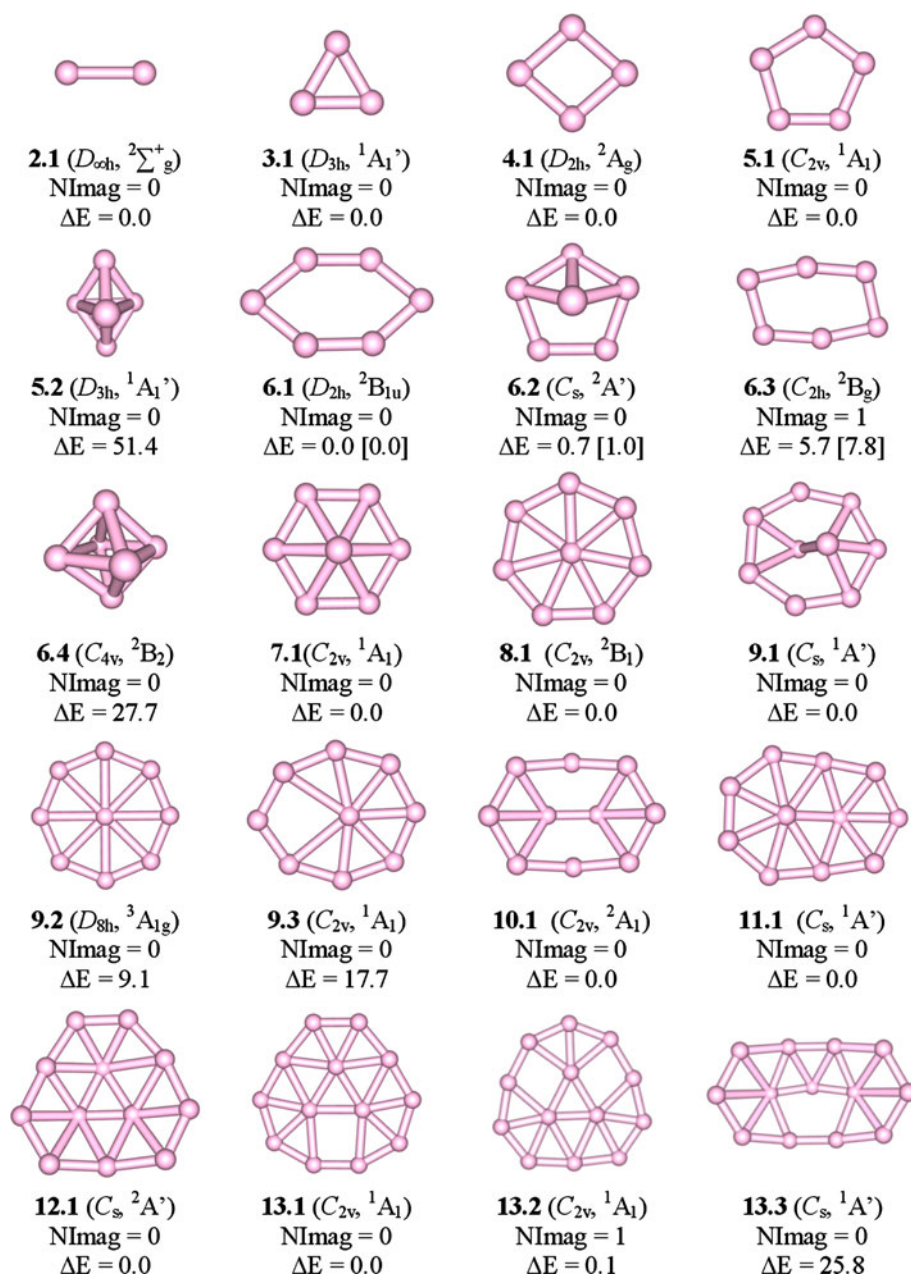
B_8^+ The C_{2v} $^2B_1$ structure **8.1** is indicated to be the most stable isomer for B_8^+ in many previous reports [36, 38–40]. Other electronic state (C_{2v} $^2A_2$) was reported by Kato et al. [34] at the MP4(SDTQ)/3-21G level. Interestingly, our calculations at the full CCSD(T)/aug-cc-pVTZ level showed that both electronic states are located having nearly the same energy content. Consequently, **8.1** is the most stable isomer of B_8^+ in both electronic states $^2B_1$ and $^2A_2$ that are apparently the two stabilized states by a Jahn–Teller distortion of a higher symmetry form.

B_9^+ Two different structures were reported as the global minimum of B_9^+. While Boustani [38] and Ricca and Bauschlicher [39, 40] found that the C_s $^1A'$ structure **9.1** is the most stable B_9^+ isomer, Kato et al. [34] showed another minimum **9.3**. Our G3B3 calculations indicate that the B_9^+ global minimum is actually the C_s $^1A'$ structure **9.1**. While the high-spin D_{8h} $^3A_{1g}$ structure **9.2** is the next isomer, **9.3** is found to be 17.7 kcal/mol less stable than **9.1**.

B_{10}^+, B_{11}^+, and B_{12}^+ Our calculations reveal that **10.1** (C_{2v}, $^2A_1$), **11.1** (C_s $^1A'$), and **12.1** (C_s, $^2A'$) are the global minima of B_{10}^+, B_{11}^+, and B_{12}^+, respectively (Fig. 3). These findings agree well with previous reports [38, 40].

B_{13}^+ The cationic cluster B_{13}^+ has been examined extensively in the literature. Anderson et al. [2]. proposed a filled icosahedron. A three-dimensional C_s structure was reported by Kawai and Weare [45] to be the most stable isomer. A distorted form of the elongated structure B_{13} was reported for B_{13}^+ by Boustani [38]. In another way, Ricca and Bauschlicher [40], Schleyer et al. [46], and Fowler and Ugalde [47] found that the global minimum of B_{13}^+ is a C_{2v} $^1A_1$ structure that is similar to its neutral. Our theoretical predictions lend a support for the assignment that the C_{2v} **13.1** structure is the most stable isomer. The other C_{2v} structure **13.2** is very close in energy to **13.1**, but it is only transition state with one imaginary frequency, whereas the C_s $^1A'$ structure **13.3** is located at 15.8 kcal/mol (Fig. 3).

Fig. 3 Shapes, electronic states, electronic states, number of imaginary frequencies (NImag), and relative energy (ΔE, kcal/mol) of the low-lying isomers B_n^+ with $n = 2$–13. The ΔE values obtained at the G3B3 approach. The values in square bracket are obtained at the CCSD(T)/aug-cc-pVTZ level

2.1 ($D_{\infty h}$, $^2\Sigma_g^+$)
NImag = 0
$\Delta E = 0.0$

3.1 (D_{3h}, $^1A_1'$)
NImag = 0
$\Delta E = 0.0$

4.1 (D_{2h}, ^2A_g)
NImag = 0
$\Delta E = 0.0$

5.1 (C_{2v}, $^1A_1$)
NImag = 0
$\Delta E = 0.0$

5.2 (D_{3h}, $^1A_1'$)
NImag = 0
$\Delta E = 51.4$

6.1 (D_{2h}, $^2B_{1u}$)
NImag = 0
$\Delta E = 0.0$ [0.0]

6.2 (C_s, $^2A'$)
NImag = 0
$\Delta E = 0.7$ [1.0]

6.3 (C_{2h}, ^2B_g)
NImag = 1
$\Delta E = 5.7$ [7.8]

6.4 (C_{4v}, $^2B_2$)
NImag = 0
$\Delta E = 27.7$

7.1 (C_{2v}, $^1A_1$)
NImag = 0
$\Delta E = 0.0$

8.1 (C_{2v}, $^2B_1$)
NImag = 0
$\Delta E = 0.0$

9.1 (C_s, $^1A'$)
NImag = 0
$\Delta E = 0.0$

9.2 (D_{8h}, $^3A_{1g}$)
NImag = 0
$\Delta E = 9.1$

9.3 (C_{2v}, $^1A_1$)
NImag = 0
$\Delta E = 17.7$

10.1 (C_{2v}, $^2A_1$)
NImag = 0
$\Delta E = 0.0$

11.1 (C_s, $^1A'$)
NImag = 0
$\Delta E = 0.0$

12.1 (C_s, $^2A'$)
NImag = 0
$\Delta E = 0.0$

13.1 (C_{2v}, $^1A_1$)
NImag = 0
$\Delta E = 0.0$

13.2 (C_{2v}, $^1A_1$)
NImag = 1
$\Delta E = 0.1$

13.3 (C_s, $^1A'$)
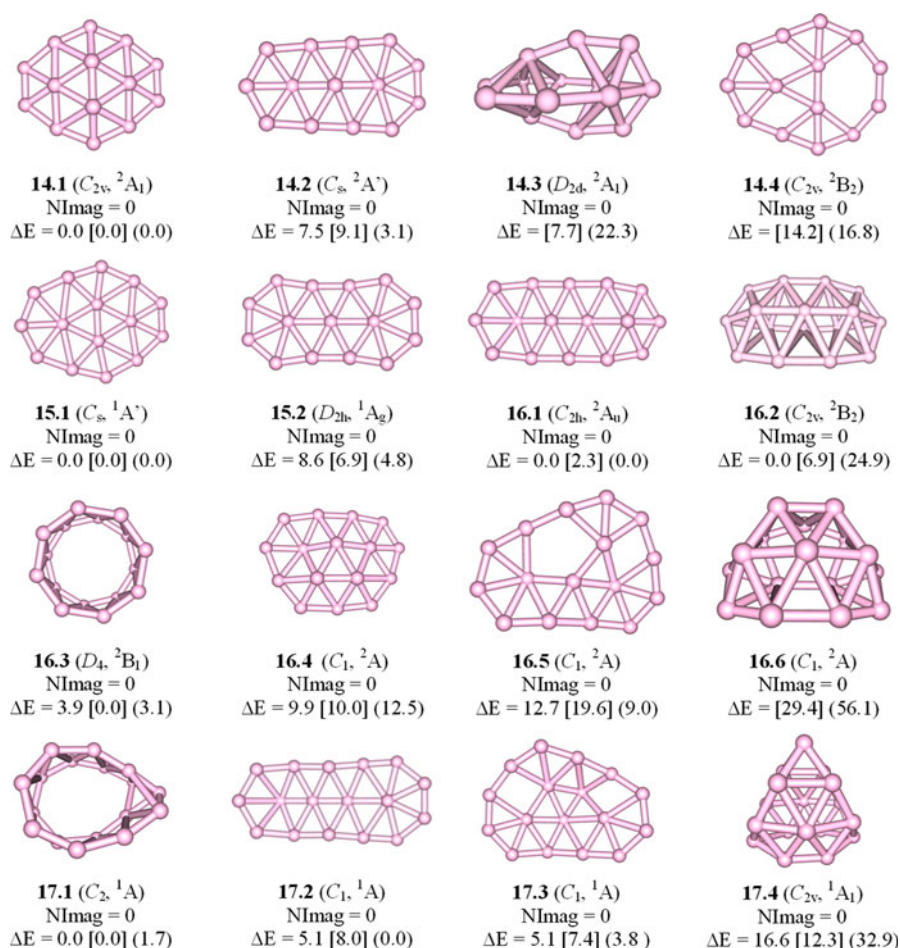NImag = 0
$\Delta E = 25.8$

The high stability of B_{13}^+ was interpreted from a MO correlation diagram [18].

B_{14}^+ and B_{15}^+ The B_n^+ systems with $n \geq 14$ have received less attention as compared to the smaller sizes. At all levels considered, our predictions concur to earlier studies [38, 40] that the C_{2v} $^2A_1$ **14.1** and C_s $^1A'$ **15.1** structures are the most stable forms of B_{14}^+ and B_{15}^+, respectively (Fig. 4).

B_{16}^+ Using the TPSS/def2-TZVPP level, Oger et al. [28] reported that the most stable isomer of B_{16}^+ is a caged form with C_{2v} symmetry **16.2**. Two structures, including an elongated form **16.1** (C_{2h} ^2A_u) and a tubular form **16.3** (D_4, $^2B_1$), are the next isomers with relative energies of 0.07 and

0.09 eV, respectively. Our BPE/6-311+G(d) results show that **16.3** is the lowest-energy isomer that is 2.3 and 6.9 kcal/mol more stable than **16.1** and **16.2**, respectively. However, B3LYP/6-311+G(d) results point out an opposite trend that **16.1** is the most stable isomer. At this level of theory, **16.2** and **16.3** are found now to be 24.9 and 3.1 kcal/mol less stable than **16.1**, respectively. Due to the difference arising from the methods employed, we further perform CCSD(T) calculations on these structures. Interestingly, our CCSD(T) results show that both structures **16.1** and **16.2** are almost degenerate with the same content in energy and 3.9 kcal/mol more stable than **16.3**. Consequently, we conclude that both structures **16.1** and **16.2** can be regarded as the degenerate lowest-energy isomers of B_{16}^+ (Fig. 4).

Fig. 4 Shapes, electronic states, number of imaginary frequencies (NImag), and relative energy (ΔE, kcal/mol) of the low-lying isomers B_n^+ with $n = 14$–17. The ΔE values obtained at the CCSD(T)/ 6-311G//B3LYP/ 6-311+G(d) level. The values in square bracket are obtained at the PBE/6-311+G(d) level. The values in parentheses are obtained at the B3LYP/6-311+G(d) level

14.1 (C_{2v}, $^2A_1$)
NImag = 0
$\Delta E = 0.0$ [0.0] (0.0)

14.2 (C_s, $^2A'$)
NImag = 0
$\Delta E = 7.5$ [9.1] (3.1)

14.3 (D_{2d}, $^2A_1$)
NImag = 0
$\Delta E = [7.7]$ (22.3)

14.4 (C_{2v}, $^2B_2$)
NImag = 0
$\Delta E = [14.2]$ (16.8)

15.1 (C_s, $^1A'$)
NImag = 0
$\Delta E = 0.0$ [0.0] (0.0)

15.2 (D_{2h}, ^1A_g)
NImag = 0
$\Delta E = 8.6$ [6.9] (4.8)

16.1 (C_{2h}, ^2A_u)
NImag = 0
$\Delta E = 0.0$ [2.3] (0.0)

16.2 (C_{2v}, $^2B_2$)
NImag = 0
$\Delta E = 0.0$ [6.9] (24.9)

16.3 (D_4, $^2B_1$)
NImag = 0
$\Delta E = 3.9$ [0.0] (3.1)

16.4 (C_1, ^2A)
NImag = 0
$\Delta E = 9.9$ [10.0] (12.5)

16.5 (C_1, ^2A)
NImag = 0
$\Delta E = 12.7$ [19.6] (9.0)

16.6 (C_1, ^2A)
NImag = 0
$\Delta E = [29.4]$ (56.1)

17.1 (C_2, ^1A)
NImag = 0
$\Delta E = 0.0$ [0.0] (1.7)

17.2 (C_1, ^1A)
NImag = 0
$\Delta E = 5.1$ [8.0] (0.0)

17.3 (C_1, ^1A)
NImag = 0
$\Delta E = 5.1$ [7.4] (3.8)

17.4 (C_{2v}, $^1A_1$)
NImag = 0
$\Delta E = 16.6$ [12.3] (32.9)

B_{17}^+ Our B3LYP/6-311+G(d) results show that two structures, including a tubular form **17.1** and an elongated **17.2**, are almost degenerate with an energy difference of 1.6 kcal/mol in favor of **17.2**. However, PBE/6-311+G(d) calculations show an opposite ordering that **17.1** is the most stable isomer and 8.0 kcal/mol more stable than **17.2**. At the higher G3B3 and CCSD(T)/6-311G(d)// B3LYP/6-311+G(d) levels, **17.1** also turns out to be the most stable isomer as showed in Fig. 4. Thus, we conclude that B_{17}^+ exhibits a C_2 ^1A global minimum **17.1**. This prediction also agrees with the earlier study by Oger et al. [28]. The C_1 ^1A structure **17.3** is the next isomer with relative energy of 5.1 kcal/mol, while 3D structure **17.4** (C_{2v}, $^1A_1$) is much less stable, as compared to other forms.
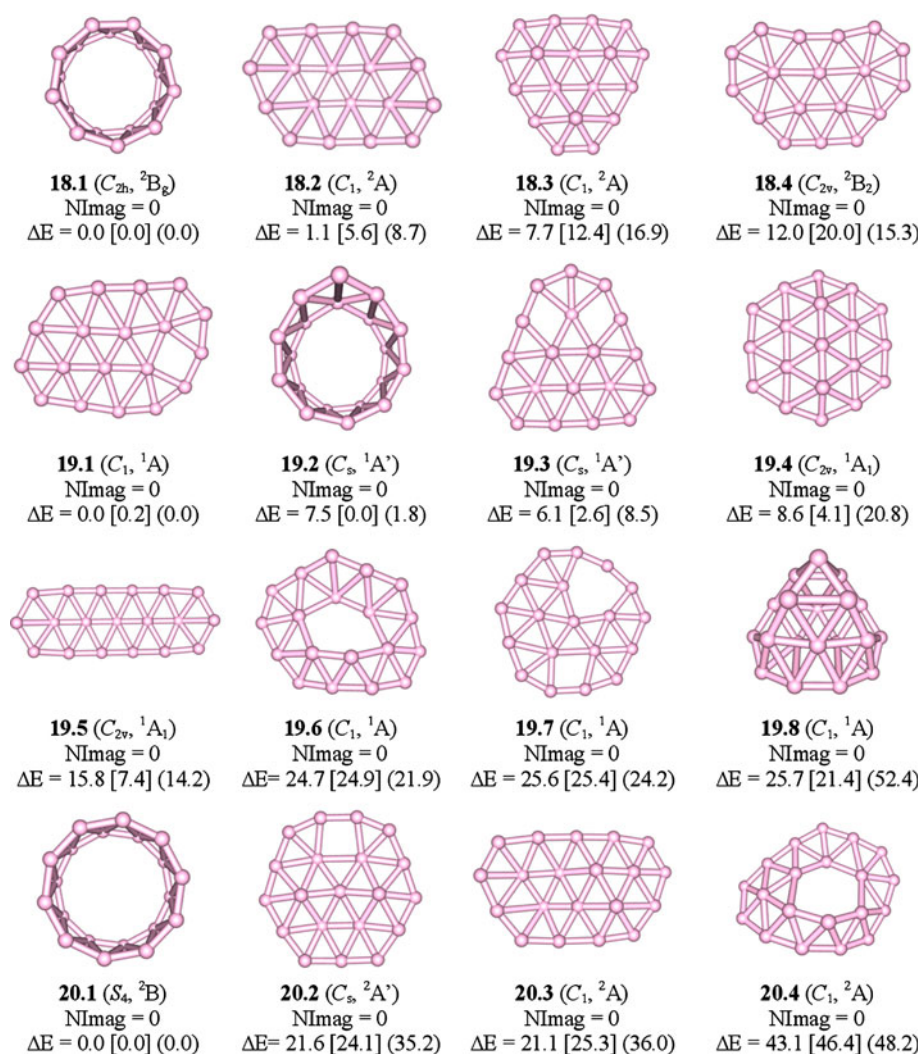
B_{18}^+ There is an interesting competition in energy between 2D and 3D structures for the B_{18}^+ species. Based on DFT calculations using two functionals B3LYP and PBE, the tubular structure **18.1** is the most stable isomer (Fig. 5). The next isomer is the quasi-planar structure **18.2** with relative energy of 5.6 and 8.7 kcal/mol at the PBE/ 6-311+G(d) and B3LYP/6-311+G(d) levels, respectively. However, this energy gap is decreased to 1.1 kcal/mol at

the CCSD(T)/6-311G(d) level. Accordingly, both structures **18.1** and **18.2** are established as the lowest-energy isomers of B_{18}^+.

18.3 is a distorted form of the neutral global minimum B_{18} and becomes the next isomer with 7.7 kcal/mol higher than **18.1**. Two other quasi-planar structures **18.4** and **18.5** are also found to be stable with relative energies of 12.0 and 15.6 kcal/mol, respectively.

B_{19}^+ There is a controversy over the identity of the B_{19}^+ global minimum. At the TPSSh/def2-TZVPP level, Oger et al. [28] reported that the most stable isomer of B_{19}^+ is a tubular form **19.2**, but it is only 0.09 eV more stable than **19.1**. Based on LDA results, Boustani et al. [29] recently showed that a 3D pyramid structure **19.8** is rather the most stable isomer for this size. In this context, we reexamine its structures using several computational methods, including three functionals B3LYP, PBE, and TPSS, and both G3B3 and CCSD(T) methods (Fig. 5). While the B3LYP and TPSS functionals provide the same trend that **19.1** is more stable but with a small energy separation of ~2.0 kcal/ mol, both structures actually have the same energy content

Fig. 5 Shapes, electronic states, number of imaginary frequencies (NImag), and relative energy (ΔE, kcal/mol) of the low-lying isomers B_n^+ with $n = 18$–20. The ΔE values obtained at the CCSD(T)/6-311G(d)//B3LYP/6-311+G(d) level. The values in square bracket are obtained at the PBE/6-311+G(d) level. The values in parentheses are obtained at the B3LYP/6-311 + G(d) level

18.1 (C_{2h}, ^2B_g)
NImag = 0
$\Delta E = 0.0$ [0.0] (0.0)

18.2 (C_1, ^2A)
NImag = 0
$\Delta E = 1.1$ [5.6] (8.7)

18.3 (C_1, ^2A)
NImag = 0
$\Delta E = 7.7$ [12.4] (16.9)

18.4 (C_{2v}, $^2B_2$)
NImag = 0
$\Delta E = 12.0$ [20.0] (15.3)

19.1 (C_1, ^1A)
NImag = 0
$\Delta E = 0.0$ [0.2] (0.0)

19.2 (C_s, $^1A'$)
NImag = 0
$\Delta E = 7.5$ [0.0] (1.8)

19.3 (C_s, $^1A'$)
NImag = 0
$\Delta E = 6.1$ [2.6] (8.5)

19.4 (C_{2v}, $^1A_1$)
NImag = 0
$\Delta E = 8.6$ [4.1] (20.8)

19.5 (C_{2v}, $^1A_1$)
NImag = 0
$\Delta E = 15.8$ [7.4] (14.2)

19.6 (C_1, ^1A)
NImag = 0
$\Delta E= 24.7$ [24.9] (21.9)

19.7 (C_1, ^1A)
NImag = 0
$\Delta E = 25.6$ [25.4] (24.2)

19.8 (C_1, ^1A)
NImag = 0
$\Delta E = 25.7$ [21.4] (52.4)

20.1 (S_4, ^2B)
NImag = 0
$\Delta E = 0.0$ [0.0] (0.0)

20.2 (C_s, $^2A'$)
NImag = 0
$\Delta E= 21.6$ [24.1] (35.2)

20.3 (C_1, ^2A)
NImag = 0
$\Delta E = 21.1$ [25.3] (36.0)

20.4 (C_1, ^2A)
NImag = 0
$\Delta E = 43.1$ [46.4] (48.2)

by PBE calculations. At higher levels, CCSD(T) results point out that **19.1** is the global minimum, being 7.5 kcal/mol more stable than **19.2**. G3B3 calculations also provide the same prediction. G3B3 energies indicate a difference of 6.3 kcal/mol in favor of **19.1**. Consequently, we conclude that the planar structure **19.1** is the global minimum of B_{19}^+.

It is surprising that while some other planar isomers **19.3**–**19.7** are found to be quite low in energy, the 3D pyramid structure **19.8** is much less stable, in contrast to the recent LDA results. This discrepancy can be understood by the fact that the LDA method is not suitable for treatment of boron clusters.

B_{20}^+ Our calculations concur with previous report that the 3D tubular structure **20.1** is the most stable isomer for B_{20}^+. Although some other isomers are also located, they are much less stable, being at least 36.0 kcal/mol higher in energy.

Generally, a structural transition in going from two-dimensional to three-dimensional forms is found to occur for this series at the B_{16}^+–B_{19}^+ sizes. While smaller B_n^+ species with $n \leq 15$ are planar or quasi-planar, a structural competition becomes effective within the intermediate sizes of B_{16-19}^+. The B_{20}^+ is clearly characterized as a 3D tubular structure. Compared to the neutral and anionic counterparts whose shapes were previously reported [27], it seems that while addition of one excess electron tends to extend the planar feature of anionic clusters, detachment of one electron from the neutrals turns out to increase the three-dimensional structural feature of cationic clusters B_n^+.

3.3 Energetic and thermochemical properties

While the different components obtained in the CBS protocol for evaluating total atomization energies (ΣD_0) of the B_n^+ cations are given in Table 2, the corresponding heats of

Table 2 CCSD(T)/CBS total atomization energies (ΣD_0, TAE, kcal/mol) for the cationic B_n^+ clusters ($n = 1$–8) and the different components

Structure	ΔCBS^a	ΔE_{ZPE}^b	ΔE_{CV}^c	ΔE_{SR}^d	ΔE_{SO}^e	ΣD_0 TAE (0 K)
B_2^+ ($^2\sum_g^+$)	−146.82	0.62	−0.52	0.03	0.06	−147.88
B_3^+ ($^1A_1'$)	−31.05	4.30	1.51	−0.13	0.09	−33.88
B_4^+ (^2A_g)	90.77	6.98	3.39	−0.26	0.12	87.03
B_5^+ ($^1A_1$)	230.26	9.13	4.10	−0.27	0.15	225.10
B_6^+ ($^2B_{1u}$)	326.39	11.33	5.25	−0.36	0.18	320.13
B_6^+ ($^2A'$)	327.26	12.62	5.89	−0.43	0.18	320.27
B_7^+ ($^1A_1$)	480.34	16.50	7.25	−0.50	0.21	470.80
B_8^+ ($^2A_2$)	600.21	16.87	8.26	−0.55	0.24	591.29

[a] Extrapolated by using Eq. (1) with the aVDZ, aVTZ, and aVQZ basis sets

[b] Zero-point energies taken from the CCSD(T) harmonic frequencies for small clusters B_n^+ ($n = 2$–6) and the MP2 harmonic frequencies for larger clusters B_n^+ ($n = 7$–8)

[c] Core-valence corrections obtained with the aug-cc-pwCVTZ basis sets at the optimized CCSD(T) geometries

[d] Scalar relativistic correction based on a CCSD(T)-DK/cc-pVTZ-DK calculation and is expressed relative to the CCSD(T) result without the DK correction

[e] Correction due to the incorrect treatment of the atomic asymptotes as an average of spin multiplets. Values based on C. Moore's Tables, Ref. [74]

Table 3 Heats of formation at 0 K [$\Delta_f H$ (0 K)] and 298 K [$\Delta_f H$ (298 K)] (kcal/mol) and average binding energies (E_b, eV) of the lowest-lying isomers B_n^+ obtained using G3B3 and CCSD(T)/CBS approaches

Structure	Label	$\Delta_f H$ (0 K)		$\Delta_f H$ (298 K)		E_b
		CBS	G3B3	CBS	G3B3	G3B3
B_2^+ ($^2\sum_g^+$)	**2.1**	418.1	421.6	419.8	423.1	0.84
B_3^+ ($^1A_1'$)	**3.2**	439.2	437.6	440.8	439.2	2.28
B_4^+ (^2A_g)	**4.1**	453.4	454.2	455.3	456.1	2.99
B_5^+ ($^1A_1$)	**5.1**	450.4	449.7	452.4	452.4	3.60
B_6^+ ($^2B_{1u}$)	**6.1**	490.5	489.6	492.6	492.2	3.69
B_6^+ ($^2A'$)	**6.2**	490.3	490.3	492.1	492.2	3.69
B_7^+ ($^1A_1$)	**7.1**	474.9	474.0	476.6	475.8	4.10
B_8^+ ($^2A_2$)	**8.1**	489.5	486.4	491.7	489.2	4.25
B_9^+ ($^1A'$)	**9.1**	–	506.9	–	509.4	4.33
B_{10}^+ ($^2B_1$)	**10.1**	–	511.2	–	513.6	4.47
B_{11}^+ ($^1A'$)	**11.1**	–	517.9	–	520.9	4.57
B_{12}^+ (^2A)	**12.1**	–	538.8	–	541.6	4.60
B_{13}^+ ($^1A_1$)	**13.1**	–	535.1	–	538.6	4.71
B_{14}^+ ($^2A_1$)	**14.1**	–	567.6	–	570.6	4.69
B_{15}^+ ($^1A_1$)	**15.1**	–	577.2	–	581.2	4.74
B_{16}^+ (^2A_u)	**16.1**	–	605.9	–	609.8	4.73
B_{17}^+ (^1A)	**17.1**	–	614.2	–	617.5	4.78
B_{17}^+ (^1A)	**17.2**	–	622.4	–	626.7	–
B_{17}^+ (^1A)	**17.3**	–	621.1	–	625.3	–
B_{18}^+ (^2B_g)	**18.1**	–	628.8	–	632.4	4.80
B_{19}^+ ($^1A'$)	**19.1**	–	641.8	–	645.8	4.83
B_{20}^+ (^2B)	**20.1**	–	646.4	–	649.9	4.87

formation at 0 and 298 K calculated from the CBS and G3B3 energies are summarized in Table 3. Adiabatic ionization energies (IEs) of the neutral clusters are calculated as the difference between heats of formation of neutral and cationic clusters at the same computational methods, and the results are shown in Table 4.

The heats of formation of neutral boron clusters B_n are taken from our previous reports [20, 26]. At the first glance,

there are small differences between heats of formation obtained from CCSD(T)/CBS and G3B3 energies. The largest difference is found to be 3.5 kcal/mol for diatomic B_2^+, while the others vary in the range of 0.7–3.1 kcal/mol. Similar observations were also found in our earlier reports on the neutral and anionic boron clusters $B_n^{0/-}$. Consequently, the heats of formation of the larger sizes B_n with $n \geq 9$ are only calculated using the composite G3B3 method.

The adiabatic ionization energies (IE) of the clusters B_n are calculated from the heats of formation of neutrals and corresponding cations obtained from both G3B3 and CCSD(T)/CBS approaches. The results are given in Table 4, together with some previous theoretical predictions and available experimental values. Small differences between the G3B3 and CBS values can again be noticed. Compared to the earlier theoretical predictions, the present G3B3 results reveal a better agreement with the available experimental data. While the IE values obtained by Boustani et al. [21] are systematically smaller than our calculated results, the MP4 values reported in Ref. [40] are much different. This discrepancy is due to the fact that the structures located in Ref. [40] differ significantly from our present structures, as discussed in a preceding section.

3.4 Relative stability of clusters

The relative stability of the B_n^+ clusters can be approached by using energetic parameters such as the average binding energy (E_b) and second-order difference in total energies ($\Delta^2 E$). These energetic properties can be defined as follows:

$$E_b(B_n^+) = [(n-1)E(B) + E(B^+) - E(B_n^+)]/n \quad (3)$$

$$\Delta^2 E(B_n^+) = E(B_{n-1}^+) + E(B_{n+1}^+) - 2E(B_n^+) \quad (4)$$

where $E(B)$, $E(B^+)$ and $E(B_n^+)$ are the total energies of B-atom, cation B^+, and B_n^+ cluster obtained at the G3B3 approach, respectively.

While the plots of these energetic parameters are displayed in Fig. 6, together with those of their corresponding neutrals for the purpose of comparison, the calculated values are given in Table 3. The average binding energy (E_b) of cationic clusters B_n^+ uniformly increases with increasing size of clusters (Fig. 6a). Similar to the trend of neutrals B_n, the highest E_b value is found for the B_{20}^+ cation. The E_b values of smaller cationic clusters B_n^+ ($n \leq 6$) are slightly smaller than those of corresponding neutral B_n. However, at larger sizes in both cationic and neutral states, the E_b values are approximately close to

Table 4 Adiabatic ionization energies (IE$_a$, eV) of boron clusters B_n obtained using G3B3 and CBS approaches

Ion structure	Neutral structure	G3B3	CBS	B3LYP[a]	MP4[b]	Exptl[c]	
B_2^+ ($^2\Sigma_g^+$)	B_2 ($D_{\infty h}$, $^3\Sigma_g^-$)	9.41	9.20	8.734	6.813	10.4	10.3
B_3^+ ($^1A_1'$)	B_3 (D_{3h}, $^2A_1'$)	9.87	9.93	9.199	8.960	9.70	14.0
B_4^+ (^2A_g)	B_4 (D_{2h}, ^1A_g)	9.86	9.92	9.813	14.390	9.80	11.8
B_5^+ ($^1A_1$)	B_5 (C_{2v}, $^2B_2$)	8.45	8.62	9.430	7.240	8.10	7.8
B_6^+ ($^2A'$)	B_6 (C_{5v}, $^1A_1$)	8.89	9.15	8.439	8.841	7.80	9.1
B_6^+ ($^2B_{1u}$)	B_6 (C_{2h}, ^3A_u)	8.59	8.82				
B_7^+ ($^1A_1$)	B_7 (C_{2v}, $^2B_2$)	8.13	8.36	7.955			
B_8^+ ($^2A_2$)	B_8 (D_{7h}, $^3A_2'$)	8.72	8.97	8.625			
B_9^+ ($^1A'$)	B_9 (C_{2v}, $^2A_1$)	8.46		8.112			
B_{10}^+ ($^2B_1$)	B_{10} (C_{2h}, ^1A_g)	8.61		8.685			
B_{11}^+ ($^1A'$)	B_{11} (C_{2v}, $^2B_2$)	8.01		7.993			
B_{12}^+ (^2A)	B_{12} (C_{3v}, $^1A_1$)	8.91		8.684			
B_{13}^+ ($^1A_1$)	B_{13} (C_s, $^2A''$)	7.24		7.941			
B_{14}^+ ($^2A_1$)	B_{14} (C_{2v}, $^1A_1$)	8.11					
B_{15}^+ ($^1A_1$)	B_{15} (C_1, ^2A)	7.39					
B_{16}^+ (^2A_u)	B_{16} (C_{2h}, ^1A_g)	8.07					
B_{17}^+ (^1A)	B_{17} (C_1, ^2A)	7.55					
B_{18}^+ (^2B_g)	B_{18} (C_{3v}, $^1A_1$)	8.05					
B_{19}^+ (^1A)	B_{19} (C_s, $^2A'$)	7.38					
B_{20}^+ (^2B)	B_{20} (D_{10d}, $^1A_{1g}$)	7.53					

[a] Theoretical values at the B3LYP/6-311+G(d) level obtained from Ref. [21]

[b] Theoretical values at the MP4/3-21G(d) level obtained from Ref. [21]

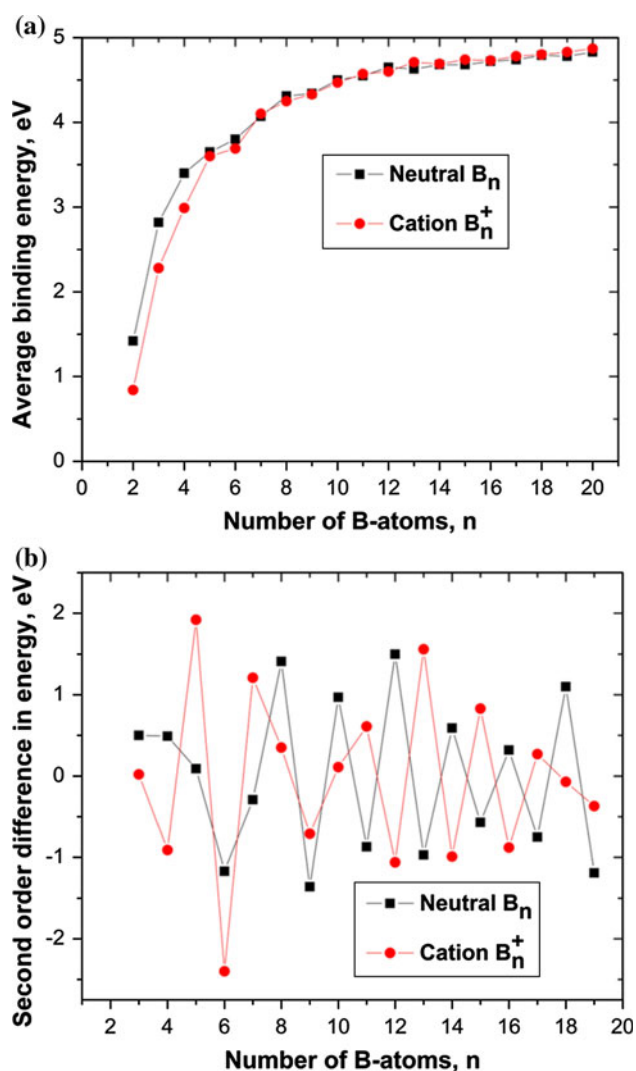[c] Experimental values obtained from Ref. [2]

Fig. 6 Average binding energy (E_b, eV) and second-order difference in total energy ($\Delta^2 E$, eV) of the B_n^+ clusters using the composite G3B3 method. The E_b and $\Delta^2 E$ values of neutral boron cluster B_n ($n = 2$–20) obtained from Refs. [20] and [26]

each other. In the cases of $n \geq 13$, the E_b values of cations B_n^+ becomes even larger than those of the neutral B_n.

The second-order difference in total energy ($\Delta^2 E$) can be considered as a measure of relative stability of clusters. Accordingly, a high value of $\Delta^2 E$ indicates a higher stability of the size as compared to its two left and right neighbors. From Fig. 6b, a consistent odd–even oscillation is easily found for the curves of $\Delta^2 E$. The closed-shell systems with an odd number of B-atoms for cation B_n^+ (with even number of B-atoms for neutral B_n) reveal local maximum peaks. Interestingly, the $\Delta^2 E$ plot of cationic clusters B_n^+ shows the enhanced peaks at $n = 5$ and 13, while the closed-shell systems B_9^+ and B_{19}^+ correspond to local minimum peaks. These observations are consistent with experimental results of mass spectroscopy previously

reported that the B_5^+ and B_{13}^+ are enhanced stability systems with high intensity peaks, whereas the low intensity peaks were found at sizes of $n = 9$ and 19 [2].

3.5 Dissociation energies (D_e)

In order to probe further the thermodynamic stability, the dissociation energies (D_e) for various fragmentation channels of the clusters are considered.

The dissociation energies for the channels $B_n^+ \rightarrow B_{n-m}^+ + B_m$ with $1 \leq m \leq n$ is defined in Eq. (3) where $\Delta_f H^0 (B_n)$ and $\Delta_f H^0 (B_n^+)$ are the heats of formation at 0 K of the B_n and B_n^+ clusters, respectively:

$$D_e \left(B_n^+ \right) = \Delta_f H^0 \left(B_{n-m}^+ \right) + \Delta_f H^0 \left(B_m \right) - \Delta_f H^0 \left(B_n^+ \right) \quad (5)$$

The smaller D_e values are found for either the fragmentation channel $B_n^+ \rightarrow B_{n-1} + B^+$ or $B_n^+ \rightarrow B_{n-1}^+ + B$ (cf. Table 5). This indicates that a B_n^+ cluster tends to decompose to form either smaller clusters B_{n-1} plus the B^+ radical or smaller cations B_{n-1}^+ plus the B-atom. Both fragmentation channels are competitive. Additionally, an odd–oven oscillation can be found for the plots of two these fragment channels (Fig. 7). The closed-shell systems B_n^+ with odd number of B-atoms reveal maximum local peaks. An exception is also found for B_9^+ whose D_e value is smaller than that of its two open-shell neighbors. This exception is consistent with the above discussions for the lower stability of B_9^+.

More interestingly is perhaps the finding that the D_e values for the fragmentation channel $B_n^+ \rightarrow B_{n-1} + B^+$ are smaller than those for the channel $B_n^+ \rightarrow B_{n-1}^+ + B$ in the cases of small clusters B_n^+ with $n \leq 11$ (cf. Fig. 7). However, for larger sizes of $n \geq 14$, an opposite trend can be found that the latter channel is more favored. These observations are consistent with our E_b predictions that the binding energy of large clusters B_n^+ ($n \geq 13$) are higher as compared to those of their corresponding neutral species.

3.6 Electron delocalization and aromaticity of cationic clusters B_n^+

Aromaticity is no doubt one of the most interesting features of small boron clusters. Possessing planar structures, these boron clusters were characterized as highly aromatic systems, on the basis of various indices such as nucleus-independent chemical shift (NICS), electron localization function (ELF), resonance energy (RE), the presence of ring current induced by an external magnetic field, and the classical Hückel rule of ($4 N + 2$) valence electrons, etc… [8–10, 27]. In recent reports [20, 26], we found that all small boron clusters B_n with $n \leq 20$ have an aromatic character, irrespective of their numbers of valence electrons.

Table 5 Dissociation energies (D_e eV) for various fragmentation channels of cationic boron clusters B_n^+ obtained using G3B3 calculations

n	D_e (1)	D_e (2)	D_e (3)	D_e (4)	D_e (5)	D_e (6)	D_e (7)	D_e (8)	D_e (9)	D_e (10)
2	1.67					1.67				
3	5.16	3.99				3.99	5.16			
4	5.14	7.45	3.50			3.50	7.45	5.14		
5	6.05	8.34	7.88	4.42		4.42	7.88	8.34	6.05	
6	4.13	7.33	6.85	6.88	3.92	3.92	6.88	6.85	7.33	4.13
7	6.53	7.82	8.24	8.26	8.78	5.91	8.78	8.26	8.24	7.82
8	5.32	9.01	7.51	8.44	8.94	5.43	9.56	8.94	8.44	7.51
9	4.97	7.44	8.35	7.35	8.77	4.49	8.72	9.36	8.77	7.35
10	5.67	7.79	7.49	8.90	8.39	5.45	8.49	9.23	9.90	8.39
11	5.57	8.39	7.73	7.93	9.82	5.19	9.34	8.89	9.66	9.41
12	4.95	7.67	7.72	7.56	8.24	5.17	8.48	9.14	8.71	8.56
13	6.02	8.12	8.06	8.61	8.94	5.34	9.52	9.33	10.01	8.67
14	4.45	7.62	6.95	7.39	8.42	5.45	8.12	8.81	8.64	8.41
15	5.44	7.05	7.43	7.26	8.19	5.57	9.21	8.40	9.11	8.03
16	4.61	7.21	6.03	6.92	7.24	5.46	8.51	8.67	7.87	7.67
17	5.50	7.26	7.08	6.40	7.78	5.66	9.28	8.85	9.02	7.32
18	5.23	7.88	6.86	7.18	6.99	5.91	9.21	9.35	8.93	8.20
19	5.29	7.67	7.54	7.03	7.83	5.48	9.53	9.34	9.50	8.17
20	5.66	8.10	7.70	8.07	8.05	6.52	9.46	10.03	9.86	9.11

(1) $B_n^+ \rightarrow B + B_{n-1}^+$; (2) $B_n^+ \rightarrow B_2 + B_{n-2}^+$; (3) $B_n^+ \rightarrow B_3 + B_{n-3}^+$; (4) $B_n^+ \rightarrow B_4 + B_{n-4}^+$; (5) $B_n^+ \rightarrow B_5 + B_{n-5}^+$; (6) $B_n^+ \rightarrow B^+ + B_{n-1}$; (7) $B_n^+ \rightarrow B_2^+ + B_{n-2}$; (8) $B_n^+ \rightarrow B_3^+ + B_{n-3}$; (9) $B_n^+ \rightarrow B_4^+ + B_{n-4}$; (10) $B_n^+ \rightarrow B_5^+ + B_{n-5}$
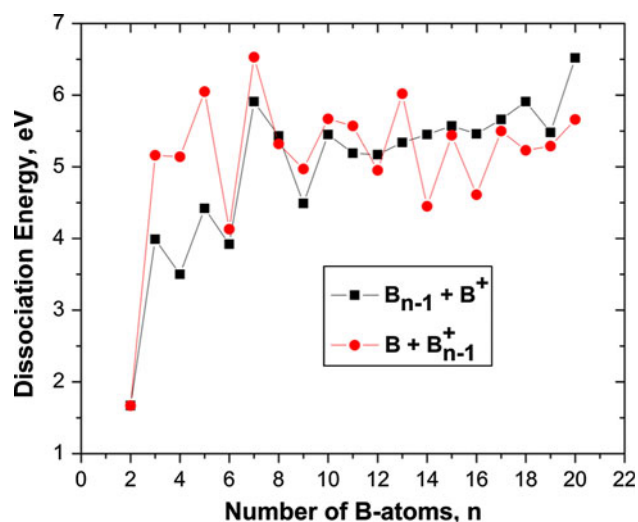
Fig. 7 Dissociation energy (D_e) of the B_n^+ clusters using the G3B3 method

In this present work, we perform an evaluation of aromaticity of closed-shell clusters B_n^+ using the NICS indices [89]. Accordingly, a compound could be regarded as aromatic when it shows negative NICS values at the ghost atoms placed on its structure. In an opposite direction, a compound is anti-aromatic when its related NICS values are positive. The NICS indices are commonly used to evaluate the aromatic features of planar cycles in the literature [8–10, 27]. Recently, it was also found to be effective for evaluating the aromaticity of three-dimensional tubular structure B_{2n} with $n = 8$–12 [90]. In this context, the NICS values of cationic boron clusters are calculated at the central positions of the global minimum structures and also at the positions of 1.0 Å on the out-plane z axis. Table 6 shows that all closed-shell species B_n^+ have an aromatic character with negative NICS values.

The electron localization of B_n^+ clusters can now be probed further by an analysis of the localized orbital locator (LOL) [91] for the enhanced stability clusters B_5^+

Table 6 NICS values of closed-shell B_n^+ cations obtained at the B3LYP/6-311+G(d) level

Structures	NICS (0,0)	NICS(0,1)
B_3^+ ($^1A_1'$)	−66.3	−17.4
B_5^+ ($^1A_1$)	−36.2	−18.8
B_7^+ ($^1A_1$)	−36.7	−23.1
B_9^+ ($^1A'$)	−23.9	−12.2
B_{11}^+ ($^1A'$)	−33.2	−20.5
B_{13}^+ ($^1A_1$)	−17.2	−20.1
B_{15}^+ ($^1A_1$)	−10.2	−5.9
B_{17}^+ (^1A)	−34.7	−27.2
B_{19}^+ (^1A)	−14.6	−12.0

and B_{13}^+. The LOL technique was proposed by Schmider and Becke [91] and is defined as follows:

$$LOL = \frac{1}{1 + \frac{\tau}{D_0}} \quad (6)$$

where τ is the local kinetic energy, D_0 is the kinetic energy in the uniform electron gas.

Consequently, high LOL values are associated with slow electrons that are characteristic of localized electrons such as electrons located in bonds or lone pairs and vice versa. Recently, the LOL indices have been effectively applied for analysis of electron delocalization of organic compounds [92, 93] and also the B_{20} cluster [20].

Our analysis of canonical molecular orbital (CMO) showed that seven valence MOs of B_5^+ are divided into two sets. The first set includes five MOs (HOMO-2, HOMO-3, HOMO-4, HOMO-5, and HOMO-6) that are responsible for five two-electron (2e)–two-center (2c) bonds between B-atoms. The two remaining MOs, including π-MO (HOMO-1) and σ-MO (HOMO) (Fig. 8a) are globally delocalized, and thus responsible for aromaticity of the B_5^+. The LOL plots for B_5^+ (Fig. 8b) reveal an internal consistence with our CMO analysis. Green-colored contractors of the first set of MOs are distributed on the B–B bonds and contribute to five 2e-2c bonds. Interestingly, the σ-LOL (in red domains) and π-LOL (in blue domains) show the contractors that are delocalized over the entire system, and thus responsible for aromaticity of B_5^+.

Similar observations are found for B_{13}^+ as shown in Fig. 9. Nineteen valence MOs can be divided into three sets. The first set of three π-MOs (HOMO-2, HOMO-3, and HOMO-8) and the second set of three σ-MOs (HOMO,
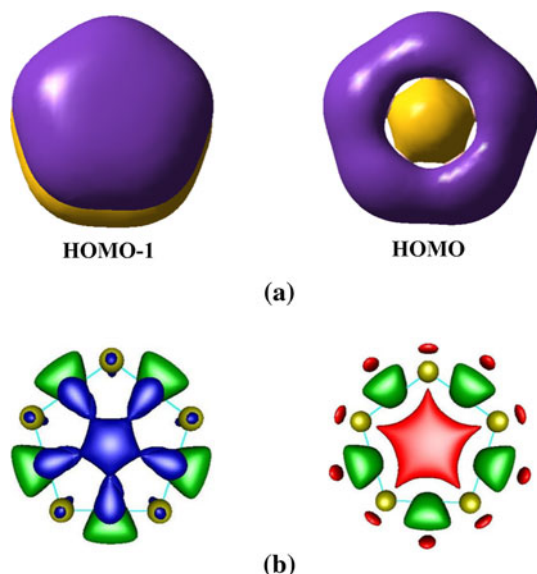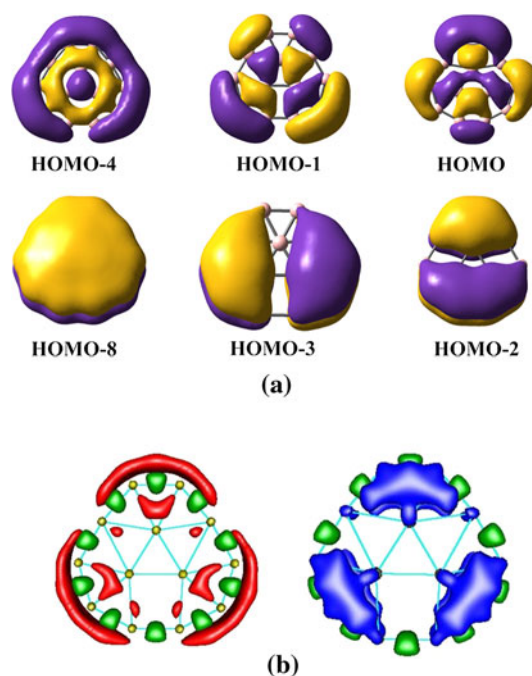

Fig. 9 a Selected MOs of the B_{13}^+ (C_{2v}) and **b** LOL isosurfaces of the B_{13}^+ (C_{2v}) at the LOL values of $0.67 \div 0.80$

HOMO-1, and HOMO-4) are globally delocalized, while the third set of remaining MOs are responsible for the B–B bonds of outer rings [18]. The LOL plots in Fig. 9b emphasize that the red-colored contractors of σ-LOL and blue-colored contractors of π-LOL are delocalized globally, and thereby make the B_{13}^+ cation aromatic.

4 Concluding remarks

In this study, we attempt to approach the boron conundrum in performing theoretical investigations on molecular structures and thermochemical properties of the cationic boron clusters B_n^+ with $n = 2$–20. Indeed, for these systems, inconsistent results on their structures and energies constitute a typical characteristic of the current literature.

In establishing the global minima, we use a stochastic search method along with high-accuracy quantum chemical calculations. The performance of computational methods is evaluated by using CCSD(T)/CBS energies as standard references. The following important points emerge from the calculated results:

1. There is a consistency between high-accuracy computational methods such as G3, G3B3, G4, and CCSD(T)/CBS.

2. For planar and quasi-planar structures, the relative energies obtained from seven different density functionals including B3LYP, BLYP, TPSS, TPSSh, PW91, PB86, and PBE are close to each other and

Fig. 8 a Selected MOs of the B_5^+ (C_{2v}) and **b** LOL isosurfaces of the B_5^+ (C_{2v}) at the LOL values of $0.67 \div 0.80$

can be compared to the CCSD(T)/CBS values. While the BLYP and B3LYP functionals are apparently less accurate for three-dimensional structures, the MP2 method is not reliable for boron clusters.

3. Single-point electronic energies obtained from CCSD(T) calculations with the MP2 and B3LYP geometries agree well with the CCSD(T)/CBS values based on CCSD(T) geometries. Differences in geometries between the B3LYP, MP2, and CCSD(T) methods induce negligible variations in relative energies.

4. A structural transition is found to occur in going from two-dimensional to three-dimensional forms for this series at the B_{16}^+–B_{19}^+ sizes. While smaller B_n^+ clusters with $n \leq 15$ are planar or quasi-planar, a structural competition becomes effective within the intermediate sizes of B_{16-19}^+. The cation B_{20}^+ is clearly characterized as a 3D tubular structure.

5. We determine a reliable and consistent set of standard heats of formation for the cationic boron clusters that are missing up to now. The adiabatic ionization energies can thereby be predicted. The average binding energy tends to increase with increasing size toward a certain limit. Enhanced stability is found for closed-shell systems B_5^+ and B_{13}^+; and

6. Finally, all closed-shell species B_n^+ have an aromatic character with negative NICS values. The electron delocalization of the enhanced stability systems B_5^+ and B_{13}^+ are analyzed by using the LOL index.

References

1. Hanley L, Anderson SL (1987) J Phys Chem 91:5161
2. Hanley L, Whitten JL, Anderson SL (1988) J Phys Chem 92:5803
3. Zhai HJ, Wang LS, Alexandrova AN, Boldyrev AI (2002) J Chem Phys 117:7917
4. Zhai HJ, Kiran B, Li J, Wang LS (2003) Nat Mat 2:827
5. Zhai HJ, Alexandrova AN, Birch KA, Boldyrev AI, Wang LS (2003) Angew Chem Int Ed 42:6004
6. Sergeeva AP, Zubarev DY, Zhai HJ, Boldyrev AI, Wang LS (2008) J Am Chem Soc 130:7244
7. Sergeeva AP, Averkiev BB, Zhai HJ, Boldyrev AI, Wang LS (2011) J Chem Phys 134:224304
8. Huang W, Sergeeva AP, Zhai HJ, Averkiev BB, Wang LS, Boldyrev AI (2010) Nat Chem 2:202
9. Alexandrova AN, Boldyrev AI (2004) J Phys Chem A 108:3509
10. Zubarev DY, Boldyrev AI (2006) J Comput Chem 28:251
11. Kiran B, Bulusu S, Zhai HJ, Yoo S, Cheng XC, Wang LS (2005) Proc Natl Acad Sci USA 102:961
12. Gopakumar G, Nguyen MT, Ceulemans A (2008) Chem Phys Lett 450:175
13. Ceulemans A, Muya JT, Gopakumar G, Nguyen MT (2008) Chem Phys Lett 461:226
14. Muya JT, Nguyen MT, Ceulemans A (2009) Chem Phys Lett 483:10
15. Muya JT, Gopakumar G, Nguyen MT, Ceulemans A (2011) Chem Phys Phys Chem 13:7524
16. Bean DE, Muya JT, Flower PW, Nguyen MT, Ceulemans A (2011) Chem Phys Phys Chem 13:20855
17. Nguyen MT, Matus MH, Ngan VT, Grant DJ, Dixon DA (2009) J Phys Chem A 113:4895
18. Kiran B, Gopakumar G, Nguyen MT, Kandalam AK, Jena P (2009) Inorg Chem 48:9965
19. Tai TB, Ceulemans A, Nguyen MT (2012) Chem Eur J 18:4510
20. Tai TB, Tam NM, Nguyen MT (2012) Chem Phys Lett 530:71
21. Akman N, Tas M, Ozdogan C, Boustani I (2011) Phys Rev B 84:075463
22. Boustani I (1997) Phys. Rev. B 55:16426
23. Grimes RN (2004) J Chem Edu 81:657 and references therein
24. Bean DE, Fowler PW (2009) J Phys Chem C 113:15569
25. Chacko S, Kanhere DG (2003) Phys Rev B 68:035414
26. Tai TB, Grant DJ, Nguyen MT, Dixon DA (2010) J Phys Chem A 114:994
27. Alexandrova AN, Boldyrev AI, Zhai HJ, Wang LS (2006) Coord Chem Rev 250:2811 and references therein
28. Oger E, Crawford NRM, Kelting R, Weis P, Kappes MM, Ahlrichs R (2007) Angew Chem Int Ed 46:8503
29. Boustani IB, Zhu Z, Tomanek D (2011) Phys Rev B 83:193405
30. An W, Bulusu S, Gao Y, Zeng XC (2006) J Chem Phys 124:154310
31. Pan L, Li J, Wang LS (2008) J Chem Phys 129:024302
32. Li F, Jin P, Jiang D, Wang L, Zhang SB, Zhao J, Chen Z (2012) J Chem Phys 136:074302
33. Ray AK, Howard IA, Kanal KM (1992) Phys Rev B 45:14247
34. Kato H, Yamashita K, Morokuma K (1992) Chem Phys Lett 190:361
35. Niu J, Rao BK, Jena P (1997) J Chem Phys 107:132
36. Bonacic-Koutecky V, Fantucci P, Koutecky J (1991) Chem Rev 91:1035
37. Garcia-Molina R, Heredia-Avalos S, Abril I (2000) J Phys Condens Matter 12:5519
38. Boustani I (1994) Int J Quant Chem 52:1081
39. Ricca A, Bauschlicher CW Jr (1997) J Chem Phys 106:2317
40. Ricca A, Bauschlicher CW Jr (1996) Chem Phys 208:233
41. Gillery C, Linguerri R, Rosmus P, Maier JP (2005) J Phys Chem 219:467
42. Li QS, Jin HW (2002) J Phys Chem A 106:7042
43. Li QS, Jin Q, Luo Q, Tang AC, Yu JK, Zhang HX (2003) Int J Quant Chem 94:269
44. Ma J, Li Z, Fan K, Zhou M (2003) Chem Phys Lett 372:708
45. Kawai R, Weare JH (1992) Chem Phys Lett 191:311
46. Gu FL, Yang X, Tang AC, Jiao HJ, Schleyer PVR (1998) J Comput Chem 19:203
47. Fowler JE, Ugalde JM (2000) J Phys Chem A 104:397
48. Frisch MJ, Trucks GW, Schlegel HB, Scuseria GE, Robb MA, Cheeseman JR, Montgomery JA Jr, Vreven T, Kudin KN, Burant JC, Millam JM, Iyengar SS, Tomasi J, Barone V, Mennucci B, Cossi M, Scalmani G, Rega N, Petersson GA, Nakatsuji H, Hada M, Ehara M, Toyota K, Fukuda R, Hasegawa J, Ishida M, Nakajima T, Honda Y, Kitao O, Nakai H, Klene M, Li X, Knox JE, Hratchian HP, Cross JB, Bakken V, Adamo C, Jaramillo J, Gomperts R, Stratmann RE, Yazyev O, Austin AJ, Cammi R, Pomelli C, Ochterski JW, Ayala PY, Morokuma K, Voth GA, Salvador P, Dannenberg JJ, Zakrzewski VG, Dapprich S, Daniels AD, Strain MC, Farkas O, Malick DK, Rabuck AD, Raghavachari K, Foresman JB, Ortiz JV, Cui Q, Baboul AG, Clifford S, Cioslowski J, Stefanov BB, Liu G, Liashenko A,

Piskorz P, Komaromi I, Martin RL, Fox DJ, Keith T, Al-Laham MA, Peng CY, Nanayakkara A, Challacombe M, Gill PMW, Johnson B, Chen W, Wong MW, Gonzalez C, Pople JA (2004) Gaussian 03, revision C.02, Gaussian Inc., Wallingford

49. Werner H-J, Knowles PJ, Lindh R, Manby FR, Schütz M, Celani P, Korona T, Rauhut G, Amos RD, Bernhardsson A, Berning A, Cooper DL, Deegan MJO, Dobbyn AJ, Eckert F, Hampel C, Hetzer G, Lloyd AW, McNicholas SJ, Meyer W, Mura ME, Nicklass A, Palmieri A, Pitzer R, Schumann U, Stoll H, Stone A J, Tarroni R, Thorsteinsson T (2006) MOLPRO, version 2006.1, a package of ab initio programs

50. Tai TB, Nguyen MT (2011) J Chem Theory Comput 7:1119

51. Stevens WJ, Krauss M, Basch H, Jasien PR (1992) Can J Chem 70:612

52. Baboul AG, Curtiss LA, Redfern PC (1999) J Chem Phys 110:7650

53. Becke AD (1993) J Chem Phys 98:5648

54. Lee C, Yang W, Parr RG (1988) Phys Rev B 37:785

55. Stephens PJ, Devlin FJ, Chabalowski CF, Frisch MJ (1994) J Phys Chem 98:11623

56. Perdew JP, Burke K, Ernzerhof M (1996) Phys Rev Lett 77:3865

57. Pople JA (1980) J. Chem. Phys 72:650

58. Bartlett RJ, Musial M (2007) Rev Mod Phys 79:291 and references therein

59. Tai TB, Kadlubanski P, Roszak S, Majumdar D, Leszkzynski J, Nguyen MT (2011) Chem Phys Chem 12:2948

60. Tai TB, Nguyen MT (2012) J Comput Chem 33:800

61. Tai TB, Nhat PV, Nguyen MT, Li S, Dixon DA (2011) J Phys Chem A 115:7673

62. Rittby M, Bartlett RJ (1988) J Phys Chem 92:3033

63. Knowles PJ, Hampel C, Werner H-J (1994) J Chem Phys 99:5219

64. Deegan MJO, Knowles PJ (1994) Chem Phys Lett 227:321

65. Dunning TH (1989) J Chem Phys 90:1007

66. Kendell RA, Dunning TH, Harrison RJ (1992) J Chem Phys 96:6796

67. Peterson KA, Woon DE, Dunning TH (1994) J Chem Phys 100:7410

68. Helgaker T, Klopper W, Koch H, Nagel J (1997) J Chem Phys 106:9639

69. Halkier A, Helgaker T, Jørgensen P, Klopper W, Koch H, Olsen J, Wilson AK (1998) Chem Phys Lett 286:243

70. Douglas M, Kroll NM (1974) Ann Phys 82:89

71. Hess BA (1985) Phys Rev A 32:756

72. Hess BA (1986) Phys Rev A 33:3742

73. De Jong WA, Harrison RJ, Dixon DA (2001) J Chem Phys 114:48

74. Moore CE (1949) Atomic energy levels as derived from the analysis of optical spectra, Volume 1, H to V; U.S. National Bureau of Standards Circular 467, U.S. Department of Commerce, National Technical Information Service, COM-72-50282: Washington, DC

75. Karton A, Martin JML (2007) J Phys Chem A 111:5936

76. Tai TB, Nguyen MT (2009) Chem Phys Lett 483:35

77. Tai TB, Nguyen MT (2010) Chem Phys 475:35

78. Tai TB, Nguyen MT, Dixon DA (2010) J Phys Chem 114:2893

79. Curtiss LA, Raghavachari K, Redfern PC, Pople JA (1997) J Chem Phys 106:1063

80. Curtiss LA, Raghavachari K, Redfern PC, Rassolov V, Pople JA (1998) J Chem Phys 109:7764

81. Curtiss LA, Redfern PC, Raghavachari K (2007) J Chem Phys 126:084108

82. Becke AD (1988) Phys Rev A 38:3098

83. Tao J, Perdew JP, Staroverov VN, Scuseria GE (2003) Phys Rev Lett 91:146401

84. Perdew JP, Kurth S, Zupan A, Blaha P (1999) Phys Rev Lett 82:2544

85. Perdew JP, Tao J, Staroverov VN, Scuseria GE (2004) J Chem Phys 120:6898

86. Perdew JP (1986) Phys Rev B 33:8822

87. Perdew JP, Burk K, Wang Y (1996) Phys Rev B 54:16533

88. Bruna PJ, Wright JS (1990) J Mol Struct Theochem 210:243

89. PvR Schleyer, Maerker C, Dransfeld A, Jiao H, Hommes NJRE (1996) J Am Chem Soc 118:6317

90. Johansson MP (2009) J Phys Chem C 113:524

91. Schmider HL, Becke AD (2000) Theochem 527:51

92. Jacobsen HJ (2009) J Comput Chem 30:1093

93. Steinmann SN, Mo Y, Corminboeuf C (2011) Phys Chem Chem Phys 13:20584